Acta Astronautica 219 (2024) 115–127

Contents lists available at ScienceDirect

Acta Astronautica

journal homepage: www.elsevier.com/locate/actaastro

Research paper

Density-based evolutionary model of the space debris environment in low-Earth orbit

Lorenzo Giudici [a,*], Camilla Colombo [a], André Horstmann [b], Francesca Letizia [b], Stijn Lemmens [b]

[a] Politecnico di Milano, Via La Masa 34, 20156, Milan, Italy

[b] European Space Agency, Robert-Bosch-Straße 5, 64293, Darmstadt, Germany

ARTICLE INFO

Keywords:
Space debris environment propagation
Continuity equation
Density distribution

ABSTRACT

Lethal untrackable debris objects pose the highest risk to the sustainability of the space environment, and thus, shall be included in the assessment of the long-term effect of mitigation and remediation measures to the space debris problem. The introduction of centimetre-sized particles in the debris evolutionary models represents a challenge from a computational cost point of view. To answer this need, this work proposes a novel probabilistic debris environment propagator. The method classifies the objects population into intact objects and fragmentation debris. The evolution of the former population is retrieved through an individual definition of each object's mission profile. A continuum approach is adopted for the characterisation of the fragments, whose density distribution in orbital elements is propagated in time through the continuity equation. The intrinsic computational efficiency of the density-based fragments cloud models is leveraged to make the method agnostic to the lowest fragments size considered. A second classification of the population of intact objects into species, such as payloads, rocket bodies, mission related objects and constellations, ensures a faithful replication of their orbit evolution. Fragmentation debris caused by intact objects explosion and accidental fragments-intact object collision are included in a probabilistic fashion at the detected fragmentation epoch, to account for their feedback effect onto the environment. The model is applied to estimate the evolution of the space debris population in low-Earth orbit up to 200 years from the reference epoch, with and without the inclusion of a future launch traffic pattern, and considering a different fulfilment of the post-mission disposal phase.

1. Introduction

Space activity is dramatically increasing and, as such, our exploitation of the space environment. Our society's growing reliance on space services on the one hand boosts the technological growth of the space sector, but on the other it is contributing to the overpopulation of some orbital regions around the Earth. Over the last ten years, the miniaturisation of space assets has played a fundamental role in this process, massively decreasing launch costs and, thus, enhancing the privatisation of the space sector. As a result, the number of satellites launched into space every year has increased from a few tens in 2011 to nearly two thousand in 2021, with communication satellites of large constellations dominating the market. Despite the sharp increase in the launch rate over the past decade, only a small fraction of the in-orbit objects population is operational [1]. At an altitude above 600 km, in the absence of a relevant sink mechanism, these inactive objects accumulate in time, causing a notable risk to the active spacecraft operations. Several studies highlighted how the untrackable debris fragments pose the highest risk, because of their intrinsic transparency to collision avoidance measures [2]. In-orbit observations, telemetry analyses and ground experiments have demonstrated how sub-centimetre particles, leveraging the high relative velocity, may seriously damage the impacted spacecraft part, or, potentially, lead to its complete destruction [3–6]. Therefore, excluding such small fragments, when establishing guidelines to address the space debris problem, results in an underestimation of the actual threat [7].

Several environment models have been developed over the years, with the aim of predicting the long-term evolution of the debris population and assessing the potential beneficial effect of remediation and mitigation measures to the space debris problem. Most of them fall in the category of the semi-deterministic approaches, as the DAMAGE (United Kingdom Space Agency) [8], DELTA (European Space Agency) [9,10], LEGEND (National Aeronautics and Space Administration) [11], LUCA (German Aerospace Centre) [12], MEDEE (National

* Corresponding author.
E-mail addresses: lorenzo1.giudici@polimi.it (L. Giudici), camilla.colombo@polimi.it (C. Colombo), andre.horstmann@ext.esa.int (A. Horstmann), francesca.letizia@esa.int (F. Letizia), stijn.lemmens@esa.int (S. Lemmens).

https://doi.org/10.1016/j.actaastro.2024.03.008
Received 16 October 2023; Received in revised form 18 January 2024; Accepted 6 March 2024
Available online 11 March 2024

Centre for Space Studies) [13], NEODEEM (Kyushu University and JAXA) [14], and SDM (Italian National Research Council) [15] software. These models describe the population of orbiting objects with a set of representative samples, whose orbit is propagated in time under the effect of any arbitrarily complex dynamics. As a result, the methods guarantee flexibility to the modelling of the debris environment in any orbital region. However, the bottleneck of the semi-deterministic models is the computational cost associated to the orbit propagation of clouds of fragments. In particular, when scaling down to the centimetre-millimetre range, to include the so-called lethal untrackable debris objects, the number of fragments grows exponentially. Furthermore, the ejected debris population becomes very diverse in both orbital parameters and physical properties, meaning that a large set of representative samples needs to be considered in order for the propagated set to accurately represent the dynamical evolution of the fragments cloud. This makes the use of semi-deterministic methods for the modelling of small fragmentation debris computationally challenging.

Alternatively, the so-called Particle-In-a-Box (PIB) models were developed [16–19]. They consider a discretisation of either the physical space or a suitable phase space into shells/volumes and derive differential equations describing the dynamics of the number of objects of different species, according to sink (e.g., atmospheric drag, active debris removal, post-mission disposal) and source (e.g., collisions and explosions) terms. Abandoning an individual characterisation of the orbiting objects, the PIB models ensure a dramatic gain from a computational cost point of view. Such advantage comes at the cost of a less accurate definition of the satellites mission profile, as well as of a simplified orbital dynamics. Nevertheless, given their efficiency compared to semi-deterministic models, they are extremely useful for a preliminary assessment of the effect of remediation and mitigation strategies on the space debris environment.

This work presents a novel long-term probabilistic debris environment propagator. The tool proposes a classification of the objects population into intact objects and fragments, and predict the evolution of the space environment up to two centuries from the reference epoch under the effect of sources, i.e., intact objects explosion and accidental fragments-intact objects collision, and sinks, i.e., atmospheric drag, mitigation and remediation measures. The intact objects population is further divided into payloads, rocket bodies, mission related objects and constellations, with each constellation treated as a separate species. This division guarantees an individual definition of the mission profile, in terms of lifetime, Post-Mission Disposal (PMD) rate, duration, and strategy, and allows to investigate the dependency of each species' environmental impact on such control parameters. A continuum approach is adopted for the characterisation of the fragmentation debris, either they belong to the background population or are generated by simulated fragmentation events. Their density distribution in orbital elements, which in the current implementation of the tool is considered as randomised in longitude of the node, argument of perigee, and mean anomaly, is propagated in time through the integration of the continuity equation. Several applications of the continuum formulation to the modelling of fragmentation clouds under different orbital regimes can be found in literature [20–24]. In [25,26], the density-based models were also extended to the propagation of the background fragments distribution in Low-Earth Orbit (LEO). The main novelty of this work is the inclusion of the continuum formulation within an elaborated debris environment propagator, with the objective of leveraging its computational efficiency. As the density-based models guarantee a computational cost which is just slightly dependent on to the lowest fragments size considered, their use allows for the potential extension of the debris evolutionary models to any objects dimension.

The paper is organised as follows:

- Section 2 presents the debris environment propagator flowchart, focusing on the logic with which the different model's building blocks are linked.
- Section 3 describes the sources from which the orbital data and physical properties of the background population are retrieved. It also explains the considered launch traffic model.
- Section 4 provides details on each model's building block.
- Section 5 presents the predictions obtained on the long-term evolution of the space environment, result of different simulation scenarios.
- Section 6 draws the conclusions of the work.

2. Model workflow

This section is devoted to explain the general structure and logic of the proposed long-term debris evolutionary model. Firstly, the methodology adopted for the division of the orbiting objects into different species, depending on their properties and control capabilities, is presented. Such classification aims at making the model flexible to the analysis of the space environmental effect of individual objects categories, as well as to the assessment of the influence of mission design parameters on the debris environment. Secondly, the debris propagator workflow is discussed. In particular, it is explained how estimates on the collision and explosion probability of orbiting objects are translated into newly generated fragments, and the way these fragmentation debris are inserted into the model as a feedback effect.

2.1. Objects classification and characterisation

The objects population is firstly divided into intact objects and fragmentation debris. This choice derives from the reasonable assumption that only intact objects may fragment into smaller pieces, and thus be a source of new fragments. It is considered that fragmentation debris do not carry any potential source of explosion, and, because of their small cross-sectional area, are not very likely to collide with each other. Furthermore, as for the vast majority of them the size is in the centimetre range [27], a potential fragmentation would result into a small net release of fragments into space. This classification is also dictated by the different philosophy adopted for describing their orbital evolution. With the objective of developing a model which is agnostic to the lowest objects dimension considered, a density-based description of the fragments dynamics is employed. Through the classical analogy with fluid dynamics, the fragmentation debris are no longer treated as single pieces, but as a fluid, whose shape and density are continuously modelled by orbital perturbations [24]. On the contrary, the orbital evolution of intact objects is individually retrieved, based on their mission profile. A detailed description of the intact objects' and fragmentation debris' orbit propagation is given in Section 4.1. It is finally worth mentioning that the proposed model only accounts for fragments-intact objects collisions. This choice is driven by the fact that only one collision between two satellites has occurred since the beginning of space exploration [1]. The introduction of such very unlikely events into a probabilistic debris evolutionary model requires further analysis and, most likely, dedicated modelling assumptions. Therefore, this part is left as a future development of the method.

The intact objects are further classified into payloads, rocket bodies, mission related objects, and constellations, with each constellation, for which at least one satellite has been launched into space, being a separate species. This division allows for an individual definition of the mission profile, in terms of lifetime, collision avoidance capability, post-mission disposal rate, duration, and strategy. The susceptibility to explosion of each category is also independently set. Note that the proposed approach makes the model flexible to the assessment of the individual contribution of each single species to the space debris problem.

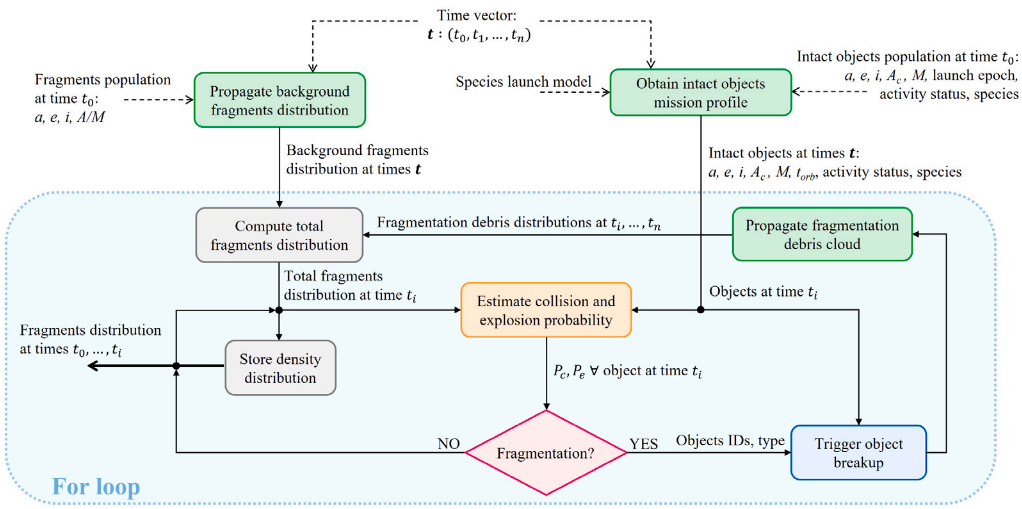

Fig. 1. Long-term debris evolutionary model flowchart. In the figure, $\boldsymbol{t}:(t_0,t_1,\dots,t_n)$ is the vector of times, a is semi-major axis, e is eccentricity, i is inclination, A/M is area-to-mass ratio, A_c is cross-sectional area, M is mass, t_{orb} is the time spent in orbit by an object since launch, P_c and P_e are collision and explosion probabilities.

2.2. Flow logic

Fig. 1 shows the flow chart of the proposed long-term debris evolutionary model. Note that this section aims at explaining the propagator workflow, while details on each of the building blocks are provided in Section 4.

As it can be observed, the model takes the following inputs:

- The background fragments population at the reference epoch, specified in terms of orbital parameters and area-to-mass ratio.
- The intact objects population at the same epoch. Orbital parameters, cross-sectional area, mass, launch epoch and species are provided for each object.
- The future launch traffic pattern. Same data as for the background intact objects population must be specified for each to-be-launched object.
- A vector of discretised times $\boldsymbol{t}$, from the reference epoch to the epoch up to which the debris evolution is monitored.

The model propagates the input populations for the time range considered, providing as output the objects coordinates at the epochs specified in $\boldsymbol{t}$. Subsequently, it iterates over the times t_i in $\boldsymbol{t}$, according to the following steps:

1. **Estimate collision and explosion probability.** The explosion and collision risk models (Sections 4.2 and 4.3) are adopted to determine the probability of breakup for each of the in-orbit intact objects at time t_i. The estimated risk is obtained based on their species properties, orbital and physical parameters, and time-in-orbit since launch t_{orb}.
2. **Fragmentation decision block.** This block decides whether to translate a value of explosion and collision probability, which is a number ranging from zero to one, into a fragmentation event. The decision is taken independently for each object, by comparing its collision, P_c, and explosion, P_e, probability with a randomly sampled number r from the uniform distribution $\mathcal{U}(0,1)$. If either $P_c > r$ or $P_e > r$, the object fragmentation is simulated. This approach has the advantage of potentially taking into consideration any debris environment evolution scenario, even if very unlikely. The main drawback is that, in order for the results to acquire statistical validity, a sufficiently high number of simulations has to be performed, and the different outcomes averaged.
3. **Trigger objects breakup.** Given as input the coordinates of the objects which successfully passed through the fragmentation decision block, the associated fragments density distributions are computed, according to fragmentations and objects type.
4. **Propagate fragmentation debris cloud.** This block computes the evolution of the fragments density distribution under the effect of the considered orbital dynamics, from time t_i to the final epoch considered, for each fragmented object.
5. **Compute total fragments distribution.** The newly generated fragments clouds are added to the background fragments distribution. The resulting population becomes the background fragments distribution for the next iteration.

At each iteration t_{i+1}, the past fragments density distribution in t_i is stored.

3. Objects population and launch traffic model

The input background fragments and intact objects populations at the reference epoch t_0 used within this work are retrieved from the DISCOS Database (Database and Information System Characterising Objects in Space) [28,29], maintained by the European Space Agency (ESA). Among other information, it provides orbital data, launch epoch and physical properties for the majority of the in-orbit tracked objects at the query epoch. In case of missing data for an object, the following steps are followed:

- If either semi-major axis or inclination are not available, the object is discarded.
- If eccentricity is not available, the orbit is assumed to be circular.
- If information on the physical properties, i.e., either mass or cross-sectional area, is missing, a different approach is employed for intact objects and fragments. For intact objects, the missing data are filled according to one of the following equations:

$$
\begin{cases}
A_c = \overline{A/M}^{(s)} M & \text{if } A_c \text{ n/a} \\
M = \dfrac{A_c}{\overline{A/M}^{(s)}} & \text{if } M \text{ n/a} \\
A_c,\ M = \overline{A_c}^{(s)},\ \overline{M}^{(s)} & \text{if } A_c, M \text{ n/a}
\end{cases}
\tag{1}
$$

where $\overline{A_c}^{(s)}$, $\overline{M}^{(s)}$, and $\overline{A/M}^{(s)}$ are the average cross-sectional area, mass and area-to-mass ratio of the species to which the intact object belongs. Instead, fragments with missing cross-sectional area or mass are assumed to be aluminium spheroids, allowing to establish a correlation between the two physical properties. As a result, if none of the two is available, the object is discarded.

The proposed long-term debris evolutionary model allows also to include a future launch traffic pattern. Following the approach proposed in [1,10], for the simulations presented in this work, new launches repeat the 2017–2021 traffic pattern, excluding constellation launches. The non-constellation objects released throughout the simulation are included in the intact objects population file together with the background population, with the launch epoch specified in the future (i.e., after the reference epoch), according to the established traffic pattern. This approach guarantees flexibility to the potential inclusion of any launch traffic model within the debris environment propagator workflow.

A different strategy is followed for the constellation objects. Considered that a reliable prediction on the long-term deployment of new constellations is not available, future launches are only limited to the replenishment of the satellites of the already (partially-) deployed constellations. In other words, when a satellite is injected in the disposal orbit, at the end of the operational phase, a new one is assumed to be instantaneously released in the constellation operational orbit. The only exception is for partially deployed constellations, for which new launches are envisioned until full deployment is achieved. The deployment rate for each partially-deployed constellation is set based on the average launch rate the constellation had up to the reference epoch t_0.

4. Model building blocks

This section provides a detailed description of the building blocks of the long-term debris evolutionary model presented in Section 2. The objects orbit propagation is firstly addressed, showing the different methodology adopted for intact objects, background fragments population, and the newly generated fragmentation debris clouds. Secondly, the explosion and collision probability models are presented. Finally, the model used to translate the objects breakup into a density distribution in Keplerian elements is described.

4.1. Objects orbital propagator

As already mentioned in Section 2, the division between intact objects and fragments allows for a separate description of their orbital evolution. An individual propagation is carried out for each intact object, such that its mission profile can be accurately replicated. On the contrary, a density-based approach is employed to describe the fragments dynamics. Note that two different continuity equation-based models are adopted for the background fragments population and the fragmentation debris clouds. The two methods are both able to convert a Partial Differential Equation (PDE) into a set of Ordinary Differential Equations (ODEs). The first adopts the Method Of Characteristics (MOC) [30], which allows to obtain the evolution of the fragments density along some characteristic curves. The interested reader can refer to Appendix B for details on the concept of characteristic curves and on the integration of a general first-order PDE through MOC. Instead, the dynamical evolution of fragmentation debris clouds is retrieved through a Finite Volume Method (FVM) [31]. The synergistic adoption of the two models aims to reduce the computational cost associated with the objects' propagation, as well as to maximise the accuracy. The MOC best works in the description of the orbital evolution of a widespread objects' population, like the initial one, as the computational cost is not directly correlated to the dimension of the domain occupied by the modelled fragments. Indeed, samples representative of the population are taken in the region where fragments are found, and their orbit and density are propagated. The competitiveness of the FVM exponentially increases with the compactness of the debris' population under study, which makes it particularly suited for the propagation of single fragmentation clouds. The second approach introduces a different perspective to the problem. Making the analogy with fluid dynamics, the MOC falls into the category of the Lagrangian specification of the flow field, where the observer follows a fluid parcel as it moves through space and time. Instead, the FVM adopts an Eulerian approach, where the observer is fixed in a particular position through which the fluid flows as time passes. If the former method has been widely adopted for the continuum modelling of space debris [20,22,23], a unique application of the Eulerian approach can be found in literature with the work by Letizia [32], who numerically integrated the continuity equation through finite differences.

Despite a different philosophy followed for the time propagation of the three objects populations, the same dynamics equations are still considered. Since the objective of this study is the prediction of the long-term evolution of the debris environment in low-Earth orbit, it is reasonable to limit the orbital disturbances to the sole effect of atmospheric drag as a first approximation [25]. The Earth's oblateness is the only perturbation comparable to drag in magnitude; however, it acts on a shorter time scale compared to the adopted time discretisation within the long-term debris propagator, which is set to one year within this work's applications. Therefore, the fragments clouds are always assumed to be uniformly spread in a band around the Earth. Instead, solar radiation pressure and luni-solar perturbations have a limited effect below 2000 km, and thus are currently neglected. Future works will be devoted to extending the tool to include a more accurate orbital dynamics.

The effect of atmospheric drag is modelled through the superimposed King-Hele approximation proposed in [33]. The atmospheric density is described as a sum of time-dependent exponential functions, as follows.

$$\rho_s(t,h) = \sum_{p=1}^{n_p} \rho_p(t,h) = \sum_{p=1}^{n_p} \hat{\rho}_p(t) e^{-h/H_p(t)} \tag{2}$$

with n_p number of partial atmospheres. The partial reference densities, $\hat{\rho}_p$, and scale heights, H_p, are obtained from fits to the Jacchia-77 model [34], at any considered time epoch t, according to the local value of the exospheric temperature T_∞, which is strictly related to the solar radio flux at 10.7 cm, $F_{10.7}$ [33]. This latter is modelled as a time-varying sinusoidal function, whose amplitude and frequency are tuned according to the value and epoch of the solar radio flux extrema. In Fig. 2 a comparison between the superimposed exponential (red continuous line), ρ_{si}, the classical piece-wise exponential (red dashed line), ρ_{pw}, and the Jacchia (blue line), ρ_J, density profiles for an exospheric temperature of 1000 K is shown. As it can be observed, the superimposed exponential density model provides a considerable improvement in the accuracy. Furthermore, it allows to eliminate the discontinuities in the profile caused by the abrupt change in the scale height value of the piece-wise exponential model. It is worth highlighting that a smoother density profile turns out to be extremely beneficial in the numerical integration of the orbital dynamics under the effect of atmospheric drag, as it significantly reduces the number of function evaluations and, consequently, the computational time.

The secular variation of semi-major axis and eccentricity is derived as a sum of King-Hele's expressions [35], for each of the partial atmosphere ρ_p. The resulting dynamics equations can be found in [33], and are reported in Appendix A for convenience.

4.1.1. Intact objects

The intact objects population provided as input contains information on the object's launch epoch and activity status. Combined to simulation settings on each species lifetime, post-mission disposal rate, duration and strategy, this allows to accurately describe the orbital evolution of each individual object, according to the scheme reported in Fig. 3.

It is worth noting that, for the simulations presented in this work, the model discerns between active and inactive objects only based on their associated species lifetime and time spent in orbit since launch t_{orb}. This choice is driven by the fact that information on the actual activity status is missing for a considerable part of the input population.

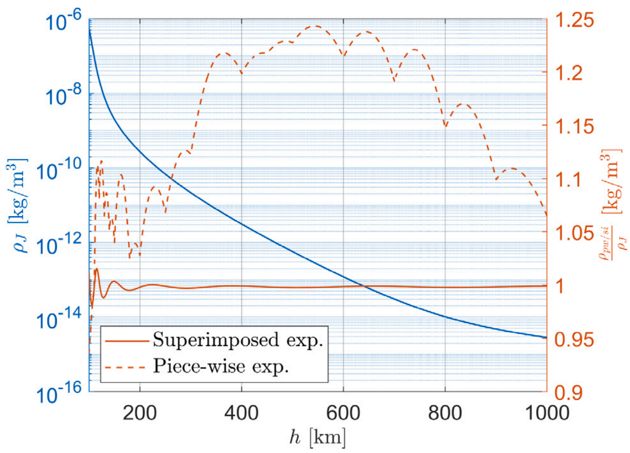

Fig. 2. Atmospheric density as function of altitude - Comparison among superimposed exponential (red continuous line), piece-wise exponential (red dashed line) and Jacchia (blue line) models. (For interpretation of the references to colour in this figure legend, the reader is referred to the web version of this article.)

However, if accurate data were provided as input, the model would already be flexible to include this additional feature.

The decision block for the post-mission disposal phase is based on the same logic adopted for the fragmentation decision block. However, in this case the random number extracted from the uniform distribution $\mathcal{U}(0,1)$ is compared against the PMD rate of the associated species. The implemented tool let the user select either circular or eccentric disposal option for each species separately. To this purpose, the King-Hele atmospheric drag theory [35] is adopted for the design of the post-mission disposal phase. According to this theory, and under the approximation of non-rotating atmosphere and exponentially decaying atmospheric density, the lifetime t_L of a satellite with semi-major axis a, eccentricity e, and area-to-mass ratio A/M is found to be [35]:

$$t_L = \begin{cases} \frac{HT(a)\eta(a)}{2\pi\delta\rho_p a^2} & \text{if } z=0 \\ \frac{e^2}{2B(a,e,\delta,\rho_p)}\left(1-\frac{11}{6}e+\frac{29}{16}e^2+\frac{7H}{8a}\right) & \text{if } 0<z\leq 3 \\ \frac{e^2}{2B'(a,e,\delta,\rho_p)}\left[1+\frac{H}{2a}\left(1-\frac{9}{20}z^2\right)\right] & \text{if } 3<z\leq 30 \end{cases} \tag{3}$$

where H is the scale height, $\delta = c_D A/M$ the inverse of the ballistic coefficient, c_D the drag coefficient, T the orbital period, ρ_p the atmospheric density at the orbit perigee, and $z := \frac{ae}{H}$. The expressions of η, B, and B' as function of the variables a, e and A/M are not reported here for brevity but can be found in [35]. Note that the expression of the lifetime t_L for $z > 30$ is not provided in Eq. (3) as associated to orbital shapes not applicable within the LEO region. Eq. (3) is transformed to be function of perigee r_p and apogee r_a radii, which allows the system to be dependent on a single independent variable r_p. Indeed:

- If **circular** PMD is selected, the apogee radius r_a^{pmd} of the disposal orbit coincides with its perigee radius r_p^{pmd}.
- If **eccentric** PMD is selected, the apogee radius r_a^{pmd} is set equal to the perigee radius r_p^{op} of the object's operational orbit.

This way, given the PMD duration, i.e., the desired object lifetime t_L after the PMD manoeuvre, Eq. (3) can be solved for r_p through a root finding algorithm. Whenever an object is already compliant with the imposed post-mission disposal duration with its operational orbit, no manoeuvre is performed and the object is let to naturally evolve under the effect of atmospheric drag. Fig. 4 depicts the necessary perigee altitude, h_p^{pmd}, to ensure atmospheric re-entry in less than 25 years as function of operational perigee altitude, h_p^{op}, and area-to-mass ratio, A/M, for both the circular and eccentric disposal options.

The discontinuity in the surfaces of solutions identifies the boundary in the $(h_p^{op}, A/M)$ domain between objects for which a manoeuvre is needed to ensure re-entry within the imposed PMD duration and those which are already compliant with their operational orbit. The solution for the circular disposal option is independent of the operational orbit perigee altitude, as the disposal orbit shares no points with the operational one. On the contrary, the eccentric disposal orbit has the apogee in correspondence of the perigee of the operational one, which induces objects operating at higher altitude to be injected on more eccentric orbits. It is worth stressing that determining the most convenient option is not an easy task and the answer might not be unique for every mission and object type, e.g., [9,12,13,15]. From the one hand the circular option avoids crossing the highly populated region at 800 km. However, the independence from the operational orbit causes a high concentration of de-orbiting objects at the same altitude, which may enhance the probability of breakup events.

4.1.2. Background fragments population

As mentioned in the introduction to this section, the distribution of the background fragments population is propagated over time through the numerical integration of the continuity equation with MOC [36]. The MOC discovers characteristic curves along which a PDE transforms into a system of ODEs (see Appendix B). For the continuity equation, the system of ODEs reads as:

$$\begin{cases} \frac{\mathrm{d}\boldsymbol{y}}{\mathrm{d}t} = \boldsymbol{F} \\ \frac{\mathrm{d}n}{\mathrm{d}t} = -n\nabla_{\boldsymbol{y}}\cdot\boldsymbol{F} \end{cases} \tag{4}$$

where $\boldsymbol{y}$ are the phase space variables, n the fragments density, and $\boldsymbol{F}$ the dynamics equations.

The fragments population at the reference epoch is interpolated through binning in the domain of Keplerian elements and area-to-mass ratio, and representative samples are extracted from the resulting distribution. Their orbit and density are eventually propagated in time, by integrating Eq. (4). In a previous work by the authors [24], the MOC for the propagation of fragmentation clouds was extended to any orbital regime. As mentioned, within this work it is limited to consider the sole effect of atmospheric drag. Because of this approximation, the propagated characteristics are interpolated through binning in a 3D space of semi-major axis a, eccentricity e, and inclination i. Instead, the fragments density is always assumed as randomised over right ascension of the ascending node Ω, argument of periapsis ω, and mean anomaly M. Note that the proposed approach is not new in space debris modelling. For instance, a similar methodology was already pursued in [37], where fragments were assigned to three-dimensional bins of semi-major axis, eccentricity and ballistic coefficient, and their density propagated.

4.1.3. Fragmentation debris

For the propagation of the newly generated fragments clouds, a FVM-based density propagator is preferred. The model, which was presented in a previous work by the authors [38], converts the continuity equation into an ODE by analytically integrating it over a control volume, in the 4D space $(a, e, i, A/M)$. For each finite volume, the integral form of the continuity equation takes the following form:

$$\frac{\mathrm{d}n}{\mathrm{d}t} = \sum_{s=1}^{2N_y}(-1)^{\left\lfloor \frac{s}{N_y}\right\rfloor}\phi_{F_i}^{(s)}, \quad i = s - \left\lfloor \frac{s}{N_y}\right\rfloor N_y \tag{5}$$

where n is the density in the given volume, N_y the number of variables, and $\phi_{F_i}^{(s)}$ the fragments flux across the s^{th} surface. Defined as $\boldsymbol{n}$ the vector of densities of all the considered volumes, the linear system of the ODEs to be integrated reads as:

$$\frac{\mathrm{d}\boldsymbol{n}}{\mathrm{d}t} = \mathcal{A}(t)\boldsymbol{n} \tag{6}$$

where the matrix $\mathcal{A}$ of time-dependent coefficients is always highly sparse, as the density equation of each control volume only depends

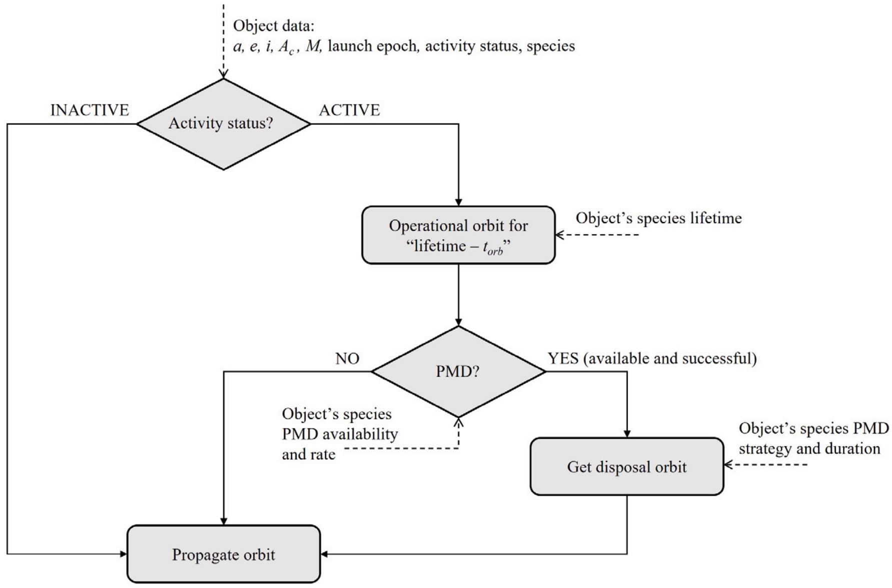

Fig. 3. Intact objects orbit propagator scheme.

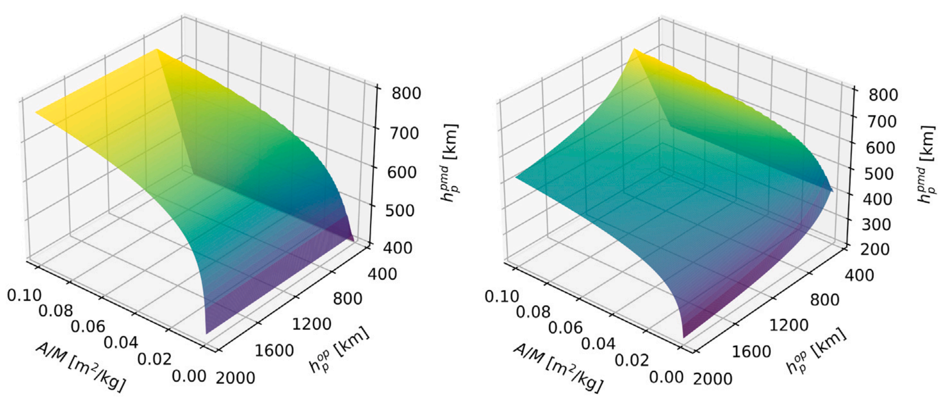

(a) Circular disposal (b) Eccentric disposal

Fig. 4. Post-mission disposal perigee altitude as function of operational perigee altitude and area-to-mass ratio.

on the density of the adjacent bins. In [38] it was shown how, under the assumption of steady atmosphere, the differential system can be integrated analytically, either via eigenvalues/eigenvectors method or through ad-hoc routines for the evaluation of the exponential of sparse arrays. With the objective of finding a compromise between accuracy and computational efficiency, the atmospheric density is here considered as a piece-wise constant function of time, i.e., the system of ODEs of Eq. (6) becomes piece-wise autonomous. By adopting the exponential matrix approach, the solution at a generic time t is found to be:

$$\boldsymbol{n}(t) = \prod_{i=0}^{N_t} \exp\left[\mathcal{A}\left(\frac{\tilde{t}+t_i}{2}\right)(\tilde{t}-t_i)\right]\boldsymbol{n}(t_0) \quad \tilde{t} = \min(t, t_{i+1}) \tag{7}$$

with N_t number of time intervals in the time range $[t_0, t)$. To further reduce the computational cost associated to each propagation, the matrix exponential is approximated through the Padè algorithm [39]. Given a generic matrix $\mathcal{M}$, it computes the matrix exponential from the solution of the following linear system of equations:

$$\mathcal{D}_{pq}(\mathcal{M})\exp(\mathcal{M}) = \mathcal{N}_{pq}(\mathcal{M}) \tag{8}$$

with:

$$\begin{aligned}\mathcal{D}_{pq}(\mathcal{M}) &= \sum_{i=0}^{p}\frac{(p+q-i)!p!}{(p+q)!(p-i)!i!}\mathcal{M}^i\\ \mathcal{N}_{pq}(\mathcal{M}) &= \sum_{i=0}^{p}\frac{(p+q-i)!q!}{(p+q)!(q-i)!i!}\mathcal{M}^i\end{aligned} \tag{9}$$

Because of the particular structure of the matrices at hand, the algorithm proves very high accuracy even stopping both expansions at the first order, i.e., setting $p = q = 1$, which dramatically contributes to improve the efficiency of the proposed cloud propagator.

4.2. Explosion probability model

The explosion probability for each intact object is defined on the basis of historical data of past fragmentation events. To this purpose, the Kaplan–Meier estimator [40] is used to determine the survival functions for the object species considered in the simulation. This estimator has been already adopted in space debris-related applications, such as in the definition of a space debris index [41,42] or in studies on active debris removal [43]. The survival function $S(t)$ is computed

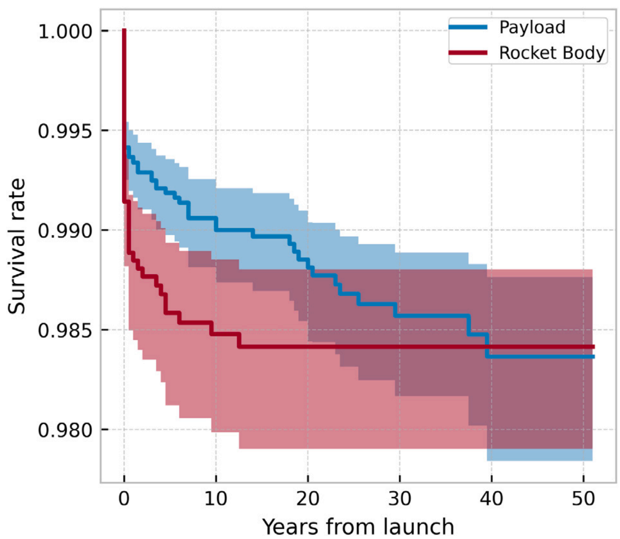

Fig. 5. Survival rate as function of time elapsed since launch for payloads and rocket bodies.

as follows.

$$S(t) = \prod_{i:\, t_i \le t} \left(1 - \frac{d_i}{n_i}\right) \tag{10}$$

with t_i a time when at least one fragmentation event has occurred, d_i the number of explosions at time t_i, and n_i the survived objects up to time t_i. From the survival function, the cumulative probability of explosion P_e after a time Δt since launch is:

$$P_e(\Delta t) = 1 - S(\Delta t) \tag{11}$$

In order for the method to be accurate, the time window over which observations are taken should be sufficiently large and comparable to the simulation time scale. As the constellations have a relatively short history, it is not reasonable to build statistics on their explosion frequency. It is also worth noting that, since the vast majority of constellation satellites are still active, no information is available for the non-operational phase. Therefore, two options are viable: the first assigns the same survival function to all payloads in the intact objects population, whether or not they belong to a constellation. The second considers constellation payloads immune from explosions. For the results presented in this paper, the second option is preferred. Mission related objects are also assumed not capable of self-fragmenting, as they do not usually carry any potential power source capable of triggering the object breakup. Fig. 5 shows the survival rate as function of time elapsed since launch for rocket bodies and payloads, obtained from the history of in-orbit explosion events until 2023. The data are retrieved from the DISCOS Database [28,29].

4.3. Collision probability model

The collision probability is modelled as a Poisson distribution [44]. Given the number of impacts η in a time range Δt, the probability of having at least one impact is defined as:

$$P_c(\Delta t) = 1 - \exp\left[-\eta(\Delta t)\right] \tag{12}$$

A fragments flux-based approach is adopted for the evaluation of the number of impacts. The impact rate is retrieved as a discrete function of time from the time-varying fragments density in Keplerian elements, as presented in a previous work by the authors [45]. Defined as $\boldsymbol{\alpha}$ the subset of elements (a, e, i), $\boldsymbol{\beta}$ the subset (Ω, ω, M), and $n_{\alpha,\beta}$ the fragments density, the impact rate $\dot{\eta}$ at a generic time t is found to be [45]:

$$\dot{\eta}(t) = A_c \iiint_{\mathbb{R}^3} \psi(\boldsymbol{\alpha}) \sum_{k=1}^{4} n_{\alpha,\beta}\left(\boldsymbol{\alpha}, \boldsymbol{\beta}^{(k)}\right) v_{\mathrm{rel}}\left(\boldsymbol{\alpha}, \boldsymbol{\beta}^{(k)}, \boldsymbol{r}_T(t)\right) \mathrm{d}\boldsymbol{\alpha} \tag{13}$$

where A_c is the intact object cross-sectional area, $\psi(\boldsymbol{\alpha})$ is the inverse of the Jacobian of the transformation from position vector $\boldsymbol{r}$ to $\boldsymbol{\beta}$, whose expression is given in [46], v_{rel} is the impact velocity, and $\boldsymbol{r}_T$ is the position vector of the target object at time t. The summation indicates the four possible solutions of intersection between a fragment orbit and the intact object, once $\boldsymbol{\alpha}$ is fixed. Note that, as the fragments density is here assumed as randomised over the angles $\boldsymbol{\beta}$, the fragments density can be taken outside of the summation as independent of $\boldsymbol{\beta}$. Thus, Eq. (13) reduces to:

$$\dot{\eta}(t) = \frac{A_c}{2\pi^3} \iiint_{\mathbb{R}^3} \psi(\boldsymbol{\alpha})\, n_{\alpha}(\boldsymbol{\alpha})\, \overline{v}_{\mathrm{rel}}\left(\boldsymbol{\alpha}, \boldsymbol{r}_T(t)\right) \mathrm{d}\boldsymbol{\alpha} \tag{14}$$

with $\overline{v}_{\mathrm{rel}}$ average impact velocity, given $\boldsymbol{\alpha}$. Note that, in Eq. (14), the density $n_{\alpha,\beta}$ is replaced by the density n_{α} in the subset of Keplerian elements $\boldsymbol{\alpha}$, according to the following relation:

$$n_{\alpha}(\boldsymbol{\alpha}) = \iiint_{\mathbb{R}^3} n_{\alpha,\beta}(\boldsymbol{\alpha})\, \mathrm{d}\boldsymbol{\beta} = 8\pi^3 n_{\alpha,\beta}(\boldsymbol{\alpha}) \tag{15}$$

as, under the approximation of randomisation in $\boldsymbol{\beta}$, each combination $(\Omega_i, \omega_i, M_i)$ over the $[0, 2\pi)$ range is equally probable. Under the assumption of piece-wise constant fragments density n_{α} and average impact velocity $\overline{v}_{\mathrm{rel}}$, Eq. (14) further simplifies as follows.

$$\dot{\eta}(t) = \frac{A_c}{2\pi^3} \sum_{i=1}^{N_b} \Psi^{(i)} n_{\alpha}^{(i)} \overline{v}_{\mathrm{rel}}^{(i)}\left(\boldsymbol{r}_T(t)\right) \tag{16}$$

where N_b is the number of bins with non-null density value and whose coordinates guarantee intersection with the intact object, and $\Psi^{(i)}$ is the integral of the function $\psi(\boldsymbol{\alpha})$ over the volume of the i^{th} bin, for which the analytical solution exists, as shown in [45]. As the impact rate is discretely evaluated over time, with a frequency much larger than the frequency of revolution of the object around the Earth, it is reasonable to compute an average impact rate over an entire intact object orbit rather than for a unique position along it. Therefore, Eq. (16) is eventually averaged over the object orbital period, as follows.

$$\overline{\dot{\eta}} = \frac{A_c}{2\pi^3 T} \sum_{i=1}^{N_b} \Psi^{(i)} n_{\alpha}^{(i)} \int_0^T \overline{v}_{\mathrm{rel}}^{(i)}\left(\boldsymbol{r}_T(t)\right) \mathrm{d}t = A_c \overline{F} \tag{17}$$

with $\overline{F}$ average fragments flux against the target object cross-sectional area over one period T. The fragments flux in 2022 as function of semi-major axis and inclination, as predicted by the proposed impact rate estimation model, according to Eq. (17), is depicted in Fig. 6. As it can be observed, the highest fragments flux value is monitored in correspondence of the highly populated region at 850–950 km altitude, at an inclination of approximately 80 degrees. As explained in [45], such inclination value guarantees the highest average relative velocity with respect to the Sun-synchronous region, where most of the fragments in LEO are found.

It is worth noticing that the average impact rate $\overline{\dot{\eta}}$ is still a function of time, as is the fragments density. However, the variation of this latter in $\boldsymbol{\alpha}$ is assumed to take place over a much larger time scale if compared to the intact object orbital period. This is the reason why $n_{\alpha}^{(i)}$ is taken outside of the time integral in Eq. (17). For each time interval Δt a single impact rate evaluation is currently implemented, in correspondence of the middle point $\hat{t}$. As a result, the number of impacts η over Δt is:

$$\eta(\Delta t) = \overline{\dot{\eta}}(\hat{t})\Delta t \tag{18}$$

4.4. Objects breakup

The estimation of the fragments density distribution as consequence of a fragmentation event is addressed in this section. The proposed model, firstly presented in [47] and improved in [24], adopts a probabilistic reformulation of the NASA Standard Breakup Model (SBM) [48,49] to bound the domain reachable by the fragments ejected by either an in-orbit collision or explosion. Such domain is primarily

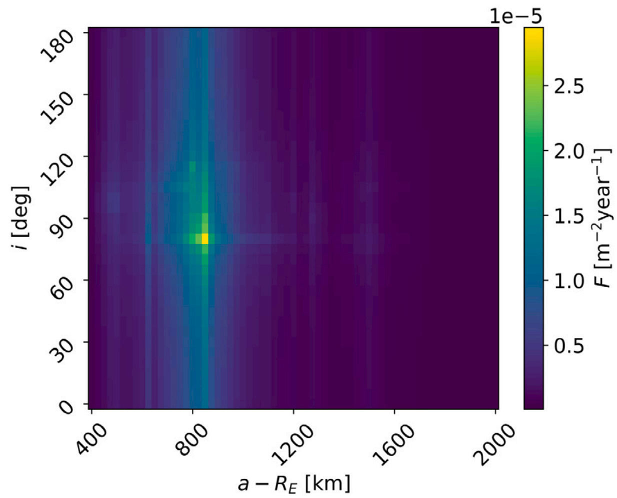

Fig. 6. Fragments (> 10 cm) flux in LEO in 2022 as function of semi-major axis and inclination.

defined in logarithm to base 10 of area-to-mass ratio, χ, and of ejection velocity, v, according to the Cumulative Density Functions (CDFs) in such variables, derived from the associated PDFs given in [49]. It is then converted into a domain in the subset of independent Keplerian elements $\boldsymbol{\alpha}$ and area-to-mass ratio A/M, by assuming the ejection velocity to be isotropically distributed in direction.

The resulting domain is eventually discretised in equally-sized rectangular-shaped volumes, through an automatised computation of the step-size in each variable, according to the average fragments density gradient over the considered domain [24]. A unique average density value is assigned to each volume, by numerically computing the integral average of the PDF in the variables $\boldsymbol{x} := (\boldsymbol{\alpha}, A/M)$, $p_{\boldsymbol{x}}$. This latter is retrieved from the original PDF in (v, χ), $p_{v,\chi}$, through change of variables [50], as follows.

$$p_{\boldsymbol{x}} = \frac{p_{v,\chi}\left(\tau^{-1}_{\boldsymbol{v}\rightarrow\boldsymbol{\alpha}}(\boldsymbol{\alpha})\right)}{\left|\det \mathrm{J}_{\boldsymbol{v}\rightarrow\boldsymbol{\alpha}}\right|} \tag{19}$$

where $\tau_{\boldsymbol{v}\rightarrow\boldsymbol{\alpha}}$ identifies the transformation from velocity vector $\boldsymbol{v}$ to $\boldsymbol{\alpha}$, and $\mathrm{J}_{\boldsymbol{v}\rightarrow\boldsymbol{\alpha}}$ is the Jacobian of the transformation, whose expression can be found in [46].

5. Simulation results

This section presents the predictions obtained on the long-term evolution of the space environment, result of different simulation scenarios. With the objective of making the results comparable with existing predictions in literature, the proposed analyses are in line with those performed with the ESA DELTA software in [1,10], with which a validation and calibration work is on-going. The three performed simulations refer to the 2022 objects population as initial one and propagate the space environment over a 200-year period. The first considers No-Further Launches (NFL) after 2022, while the other two analyses introduce the repetitive launch traffic pattern presented in Section 3. The effect of a different fulfilment of the post-mission disposal phase is also investigated. PMD success rate and duration are initially set in accordance to observed values, considering the performance for objects with End-Of-Life (EOL) equal or later than 2015 [1]. The second scenario, with launches after 2022 and observed PMD capabilities, is referred to as Extrapolation, as it extrapolates on the current behaviour in terms of both launch traffic and disposal rate. Instead, the third analysis describes a very Optimistic scenario where EOL capabilities are considerably improved with respect to current standards, to assess the severity of the space debris problem even in the most conservative case. The studied simulations scenarios are summarised in Table 1.

Table 1
List of studied simulation scenarios.

	NFL	Extrapolation	Optimistic
Launches	No	Yes	Yes
PMD orbit	Eccentric	Eccentric	Eccentric
PMD rate - P/L	0.40	0.40	0.99
PMD rate - C	0.90	0.90	0.99
PMD rate - R/B	0.55	0.55	0.99

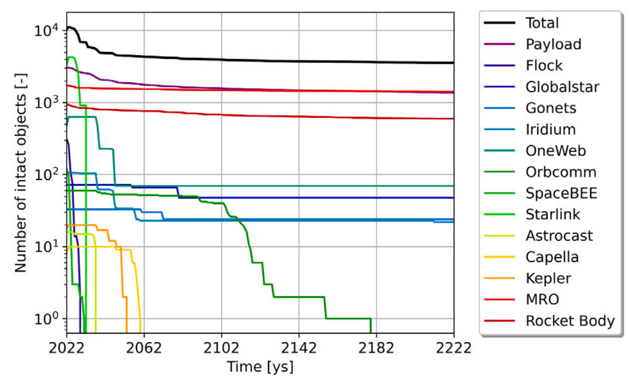

Fig. 7. Number of intact objects over time, total and per single species profiles - NFL.

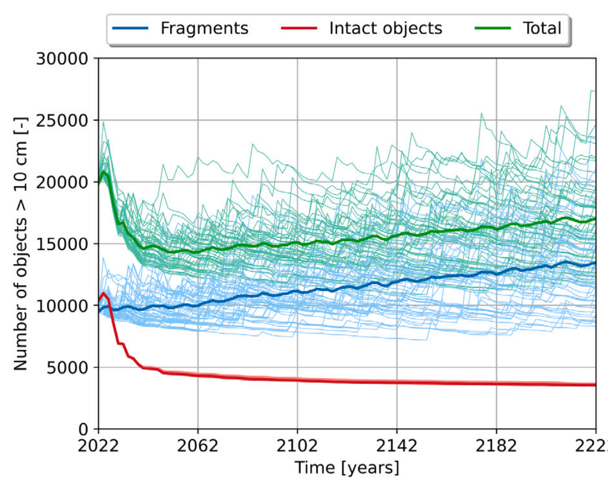

Fig. 8. Number of objects > 10 cm over time, average and per single run profiles - NFL.

For all the proposed analyses, 50 runs are performed according to the block diagram of Fig. 1, and the resulting estimates are eventually averaged.

5.1. No-further launches simulation results

Despite being an unrealistic scenario, the NFL case allows to eliminate the intrinsic uncertainty component related to the future launch traffic pattern [51], which is crucial when comparing different long-term debris evolutionary models. The outcome of this scenario describes how the space environment would evolve if space activity stopped, with the only exception of active satellites in 2022, which would accomplish their planned mission profile. Therefore, it can give a measure of the current status of the space environment, determining if the combined effect of natural decay and controlled re-entry of orbiting objects could still prevail on the fragments sources, i.e., collisions and explosions.

Fig. 7 depicts the evolution over time of the number of in-orbit intact objects of the 2022 reference population, obtained according

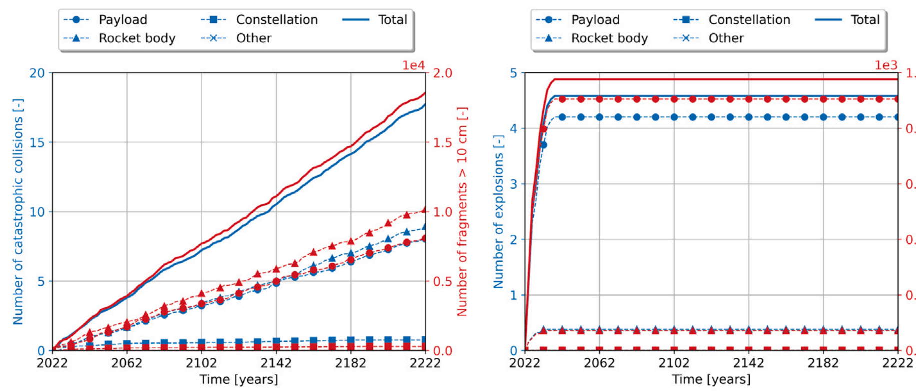

(a) Fragment-intact object catastrophic collisions.

(b) Explosions.

Fig. 9. Cumulative number of fragmentation events and fragments released into orbit over time, total and per species profiles - NFL.

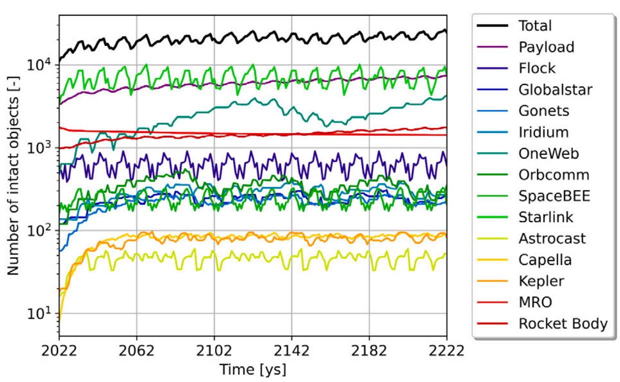

Fig. 10. Number of intact objects over time, total and per single species profiles - Extrapolation.

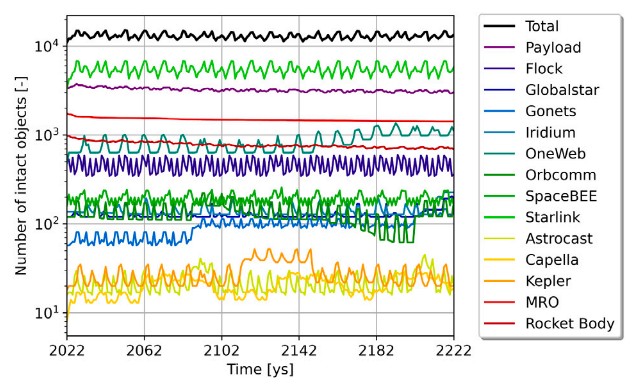

Fig. 11. Number of intact objects over time, total and per single species profiles - Optimistic.

to the scheme reported in Fig. 3, with the objects capable of performing a disposal manoeuvre following the PMD strategy reported in Table 1. As it can be observed, active constellation payloads are characterised by a similar trend, with an initial growth for partially-deployed constellations, a steady period when the objects are on either the operational or the disposal orbit, and a sudden drop at the end of the PMD phase. It is worth noticing that, as some of the constellations orbit at an altitude which guarantees natural re-entry in less than the prescribed 25 years (e.g., Starlink, SpaceBEE, Flock, Kepler, Astrocast), the PMD phase is shortened for these payloads and all the objects re-enter the atmosphere, despite the imposed PMD rate. On the contrary, the uncontrolled orbiting objects, e.g., rocket bodies and MROs, are characterised by a smooth decrease in number over time, induced by the sole effect of atmospheric drag.

Fig. 8 illustrates the predicted evolution of the number of objects larger than 10 cm over time. In order to identify the uncertainty domain of the results, both the average (thick lines) and single run (thin lines) profiles are shown. Instead, Figs. 9(a) and 9(b) depict the estimated cumulative number of fragment-intact object catastrophic collisions and explosions, respectively. The associated number of fragments injected into orbit is also shown. As it can be observed, in the absence of future launches, the model estimates a decrease in the total number of in-orbit objects over the 200-year propagation time. This behaviour is mostly induced by the sudden drop caused by the disposal of controlled objects within the first 30 years, which overcomes the release of debris from fragmentation events. Nevertheless, a constant increase of fragments is monitored, meaning that collisions and explosions would already prevail on atmospheric drag, even if space activity had stopped in 2022.

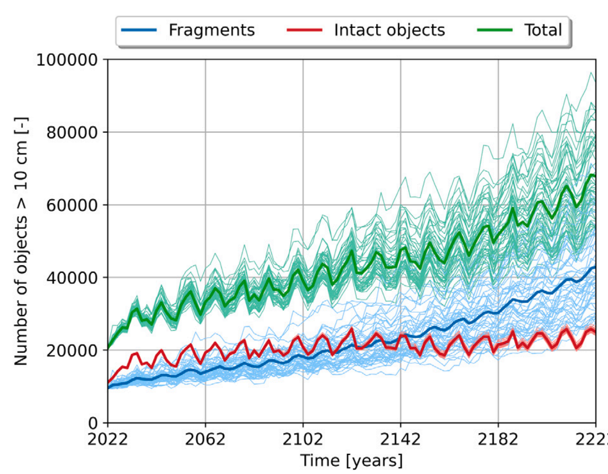

Fig. 12. Number of objects > 10 cm over time, average and per single run profiles - Extrapolation.

By looking at Fig. 9, it can be inferred that rocket bodies are on average the most likely to fragment due to a collision. Indeed, despite being outnumbered by payloads and constellations, the absence of collision avoidance capabilities makes them more susceptible to such events. On the contrary, the greater number of payloads causes this species to trigger significantly more explosions than rocket bodies, in spite of a higher average reliability (Fig. 5).

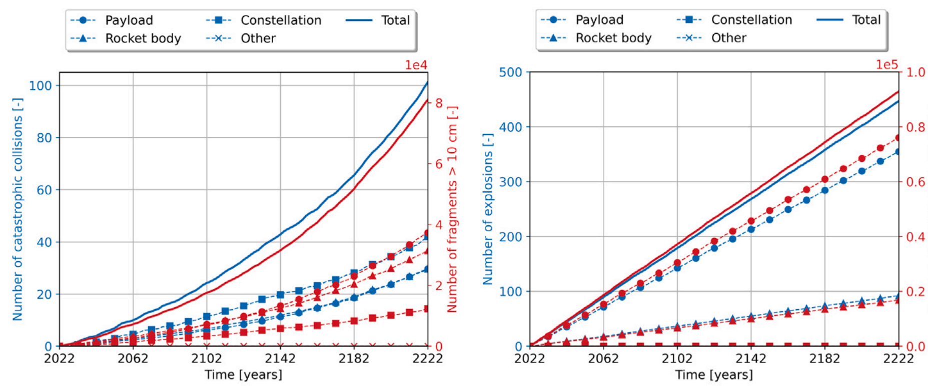

(a) Fragment-intact object catastrophic collisions.

(b) Explosions.

Fig. 13. Cumulative number of fragmentation events and fragments released into orbit over time, total and per species profiles - Extrapolation.

5.2. Repetitive launch traffic pattern simulation results

As detailed in Section 3, the implemented launch traffic model foresees the repetition of 2017–2021 traffic pattern over the 200-year propagation time for the objects not belonging to any of the constellations [1,10]. Instead, a continuous replenishment of constellation payloads is considered. The resulting evolution over time of the number of in-orbit intact objects, for the two PMD strategies reported in Table 1, are depicted in Figs. 10 and 11, respectively. As it can be seen, constellation payloads are characterised by an oscillatory profile dictated by the combined effect of the time-varying solar flux value, the lifetime of the object (different for every constellation), and the imposed post-mission disposal duration. It can be further appreciated how the 25 years PMD duration causes a greater accumulation of inactive objects in orbit; indeed, it is worth remarking that the replenishment takes place at the end of the operational phase. As a result, if the number of active payloads keeps constant, the inactive ones accumulate according to the PMD duration-lifetime ratio. The profiles of payloads and rocket bodies oscillate with an 11-year period, more evident in Fig. 10 because of the longer PMD phase, correspondent to one solar cycle. It is worth observing that such behaviour was not present in the NFL scenario of Fig. 7, even though it already considered the dependency of atmospheric density on time. The difference is caused by the fact that every 5 years the very same set of objects is here released into orbit, meaning that atmospheric drag continuously acts on a very similar satellites population but with varying magnitude, inducing the oscillatory behaviour.

Figs. 12 and 14 depict the obtained evolution of the objects number over time for the Extrapolation and Optimistic scenarios, respectively. Figs. 13 and 15 illustrate the associated cumulative number of fragment-intact object catastrophic collisions and explosions, as well as the amount of debris injected into orbit by such events. It can be immediately inferred how the very stringent PMD strategy of the Optimistic case dramatically decreases the predicted number of orbiting fragments, which are halved after 200 years. Even greater is the effect on the number of catastrophic collisions, reduced by a factor three, which from the exponential behaviour highlighted in Fig. 13(a) reduces to a linear increase in the Optimistic scenario of Fig. 15(a). It is interesting to observe that constellations, from being the most vulnerable objects species in the Extrapolation scenario from the point of view of collision events (Fig. 13(a)), are the least likely to be impact by a fragment in the case of equal and very stringent PMD rate for all species (Fig. 15(a)). This result is justified by a considerably lower number of in-orbit constellation derelict objects compared to rocket bodies and payloads. Note also that a higher number of catastrophic collisions for an object category does not necessarily translate into a larger population of fragmentation debris released into orbit, which,

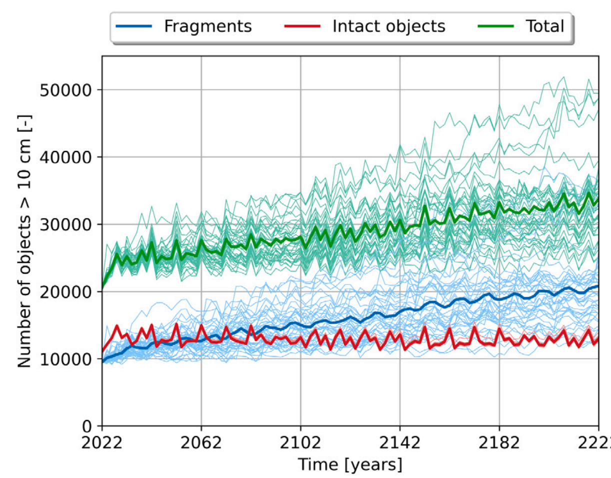

Fig. 14. Number of objects > 10 cm over time, average and per single run profiles - Optimistic.

according to the NASA SBM, strictly correlates to the objects mass [48]. Because of the significantly smaller average mass for constellation satellites compared to individual payloads and rocket bodies, the number of ejected fragments associated to this species is considerably lower.

The reduction of explosion events in the Optimistic scenario comes as a direct consequence of an average lower number of in-orbit payloads and rocket bodies, induced by a more reliable and faster deorbiting phase. It is worth observing that the number of rocket body explosions is approximately six times lower than the payload ones, which might seem in contrast with current trends in fragmentation events [52]. However, this behaviour is fully justifiable by the considered modelling assumptions and the simulation settings of the Optimistic scenario, which is far from picturing the current behaviour of the space environment. The number of explosion events depends on three main quantities. First, on the number of in-orbit objects of the given species. As already commented, rocket bodies are significantly outnumbered by payloads. Second, on the survival rate function of the given species. Since this latter is retrieved from the whole history of fragmentation events until 2023, the profile pictures the trend in explosion rate since the beginning of space activity, which can differ form the current behaviour. However, enough data are necessary to build the statistics, which implies that accurate survival functions cannot be obtained from last years' fragmentation events only. Third, on the average lifetime of an object belonging to the given species. Note that, as there is no operational phase for rocket bodies, the

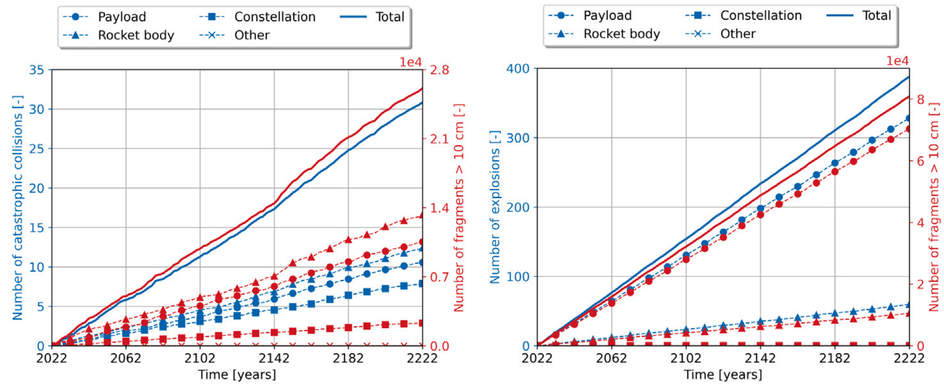

(a) Fragment-intact object catastrophic collisions.

(b) Explosions.

Fig. 15. Cumulative number of fragmentation events and fragments released into orbit over time, total and per species profiles - Optimistic.

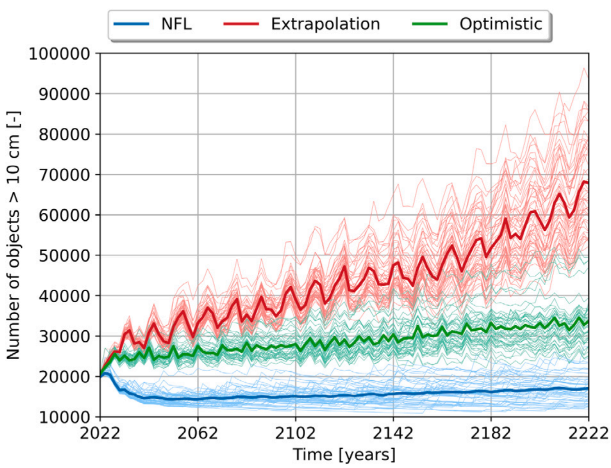

Fig. 16. Number of objects > 10 cm over time for the three considered simulation scenarios.

ones launched throughout the simulation re-enter in a time shorter or equal to the imposed post-mission disposal duration. This implies that, in the Optimistic case, all launched rocket bodies stay in orbit for maximum one year. As a result, the population of rocket bodies is mostly constituted by the background population, which was already in orbit before the reference epoch. From the plot of the survival function of Fig. 5, it can be inferred that, after 12 years from launch, rocket body explosions experience a plateau. This makes the probability of a rocket body exploding very low in the Optimistic scenario. On the contrary, as all launched payloads have an initial operational phase, they remain in orbit during the years when, according to the survival function, they are more likely to explode.

The profiles of the predicted number of in-orbit objects for the three simulation scenarios of Table 1 are finally displayed together in Fig. 16, to better highlight the relative behaviour.

6. Conclusion

Evidences prove that untrackable objects must be included in the long-term simulation of the space debris environment. This poses a challenge from a computational perspective, as the number of objects grows exponentially as size decreases. To this aim, this paper proposed a novel density-based long-term debris environment propagator. The model divides the objects population into fragmentation debris and intact objects. This classifications allows to treat the former not as single pieces but as a cloud, whose density function is propagated over time through the numerical integration of the continuity equation, in the domain of Keplerian elements and area-to-mass ratio. In particular, two continuum formulations were proposed: the background fragments population was propagated through the method of characteristics. A finite volume method was instead preferred for the newly generated fragments, because they evolve in the considered variables as a compact cloud. A second classification into 15 species was considered for the intact objects population, with the objective of characterising each object category separately in terms of post-mission disposal strategy, collision avoidance capability, and susceptibility to explosion. A statistical explosion probability model and a flux-based collision risk estimator were adopted for the introduction of fragmentation events within the propagator workflow, to account for their feedback effect.

Three 200-year simulation scenarios related to the 2022 initial objects population were eventually proposed. The analyses were performed both with and without future launches, and considering different post-mission disposal strategies. The results presented in this paper were still limited to objects larger than 10 cm, with the objective of making the tool comparable to other debris evolutionary models. However, as the density-based fragments cloud models are intrinsically agnostic to the lowest fragments size considered, future studies will be dedicated to the extension of the long-term simulation of the space debris environment to the modelling of the so-called lethal untrackable debris objects.

Declaration of competing interest

The authors declare that they have no known competing financial interests or personal relationships that could have appeared to influence the work reported in this paper.

Acknowledgements

This work was carried out within the project funded by the Italian Space Agency, Italy "Detriti Spaziali Supporto alle attività IADC e SST 2019-2021".

Appendix A. Super-imposed King-Hele atmospheric drag model

The variations of semi-major axis, a, and eccentricity, e, under the effect of atmospheric drag read as [53]:

$$\begin{aligned}\frac{\mathrm{d}a}{\mathrm{d}t} &= -\frac{a^2\rho\delta v^3}{\mu}\\ \frac{\mathrm{d}e}{\mathrm{d}t} &= -\frac{a\rho\delta v}{r}(1-e^2)\cos E\end{aligned} \tag{A.1}$$

where ρ is the atmospheric density, $\delta = c_D A/M$ is the inverse of the ballistic coefficient, r and v are the orbital radius and velocity, respectively, which can be expressed as function of semi-major axis a, eccentricity e, and eccentric anomaly E, as follows [53].

$$r = a(1 - e\cos E) \tag{A.2}$$

$$v = \sqrt{2\frac{\mu}{r} - \frac{\mu}{a}} \tag{A.3}$$

with μ planetary constant. By averaging the expressions in Eq. (A.1) over a full orbital period $T = 2\pi\sqrt{\frac{a^3}{\mu}}$, according to the formulation in [35], the following expressions are found [33]:

$$\begin{aligned}
\overline{\frac{\mathrm{d}a}{\mathrm{d}t}} &= -\frac{\delta}{2\pi}\sqrt{\mu a}\int_0^{2\pi}\rho(h)\frac{(1+e\cos E)^{\frac{3}{2}}}{(1-e\cos E)^{\frac{1}{2}}}\,\mathrm{d}E \\
\overline{\frac{\mathrm{d}e}{\mathrm{d}t}} &= -\frac{\delta}{2\pi}\sqrt{\frac{\mu}{a}}\int_0^{2\pi}\rho(h)\left(\frac{1+e\cos E}{1-e\cos E}\right)^{\frac{1}{2}}\cos E(1-e^2)\,\mathrm{d}E
\end{aligned} \tag{A.4}$$

Plugging the super-imposed atmospheric density function of Eq. (2) into Eq. (A.4), the original King-Hele contraction formulation [35] can be extended to the super-imposed King-Hele model, according to the following equations:

$$\begin{aligned}
\overline{\frac{\mathrm{d}a}{\mathrm{d}t}} &= \sum_{p=1}^{n_p}\overline{\frac{\mathrm{d}a}{\mathrm{d}t}}_p = -\frac{\delta}{2\pi}\sqrt{\mu a}\sum_{p=1}^{n_p}\int_0^{2\pi}\rho_p\frac{(1+e\cos E)^{\frac{3}{2}}}{(1-e\cos E)^{\frac{1}{2}}}\,\mathrm{d}E \\
\overline{\frac{\mathrm{d}e}{\mathrm{d}t}} &= \sum_{p=1}^{n_p}\overline{\frac{\mathrm{d}e}{\mathrm{d}t}}_p = -\frac{\delta}{2\pi}\sqrt{\frac{\mu}{a}}\sum_{p=1}^{n_p}\int_0^{2\pi}\rho_p\left(\frac{1+e\cos E}{1-e\cos E}\right)^{\frac{1}{2}}\cos E(1-e^2)\,\mathrm{d}E
\end{aligned} \tag{A.5}$$

As it can be noted, each partial contraction reduces to the original King-Hele formulation with the partial exponential atmosphere ρ_p. Therefore, the solutions of the integrals in Eq. (A.5), for different eccentricity regimes, can be found in [35].

Appendix B. Method of characteristics

A brief recap of the method of characteristics is provided here, following the outline given in [54]. Let us consider a general first-order quasi-linear partial differential equation:

$$a(x,y,u)\frac{\partial u}{\partial x} + b(x,y,u)\frac{\partial u}{\partial y} = c(x,y,u) \tag{B.1}$$

If $u := u(x,y)$ is a solution of Eq. (B.1), at every point (x,y,z) on the surface $\mathcal{S} = \{(x,y,u)\}$, the vector $[a(x,y,u), b(x,y,u), c(x,y,u)]$ lies in the tangent plane to the surface, i.e., the following condition holds:

$$[a(x,y,u), b(x,y,u), c(x,y,u)] \cdot \left[\frac{\partial u}{\partial x}, \frac{\partial u}{\partial y}, -1\right] = 0 \tag{B.2}$$

To determine the surface $\mathcal{S}$, one can construct curves $\mathcal{C}$, parametrised by s, such that at each point on the curve $\mathcal{C}$ the vector $[a(x,y,u)$, $b(x,y,u), c(x,y,u)]$ is tangent to the curve. The curve $\mathcal{C} = \{(x(s), y(s)$, $z(s))\}$ satisfies the following system of ODEs:

$$\begin{aligned}
\frac{\mathrm{d}x}{\mathrm{d}s} &= a(x(s), y(s), z(s)) \\
\frac{\mathrm{d}y}{\mathrm{d}s} &= b(x(s), y(s), z(s)) \\
\frac{\mathrm{d}z}{\mathrm{d}s} &= c(x(s), y(s), z(s))
\end{aligned} \tag{B.3}$$

The curves $\mathcal{C}$ are known as characteristic curves for Eq. (B.1). They are found by integrating the system of ODEs of Eq. (B.3).

References

[1] ESA Space Debris Office, ESA's annual space environment report, Tech. Rep., 2023.

[2] D. McKnight, T. Maclay, Space environment management: A common sense framework for controlling orbital debris risk, in: Advanced Maui Optical and Space Surveillance Technologies Conference, 2019, p. 35.

[3] G. Drolshagen, Impact effects from small size meteoroids and space debris, Adv. Space Res. 41 (2008) 1123–1131, http://dx.doi.org/10.1016/j.asr.2007.09.007.

[4] V. Adushkin, O. Aksenov, S. Veniaminov, S. Kozlov, V. Tyurenkova, The small orbital debris population and its impact on space activities and ecological safety, Acta Astronaut. 176 (2020) 591–597, http://dx.doi.org/10.1016/j.actaastro.2020.01.015.

[5] H. Krag, M. Serrano, V. Braun, P. Kuchynka, M. Catania, J. Siminski, M. Schimmerohn, X. Marc, D. Kuijper, I. Shurmer, A. O'Connell, M. Otten, I. Muñoz, J. Morales, M. Wermuth, D. McKissock, A 1 cm space debris impact onto the sentinel-1A solar array, Acta Astronaut. 137 (2017) 434–443, http://dx.doi.org/10.1016/j.actaastro.2017.05.010.

[6] N. Smirnov, A. Kiselev, M. Smirnova, V. Nikitin, Space traffic hazards from orbital debris mitigation strategies, Acta Astronaut. 109 (2015) 144–152, http://dx.doi.org/10.1016/j.actaastro.2014.09.014.

[7] A.E. White, H.G. Lewis, The many futures of active debris removal, Acta Astronaut. 95 (2014) 189–197, http://dx.doi.org/10.1016/j.actaastro.2013.11.009, URL https://www.sciencedirect.com/science/article/pii/S0094576513004013.

[8] H.G. Lewis, G. Swinerd, N. Williams, G. Gittins, DAMAGE: a dedicated GEO debris model framework, in: Proceedings of the 3rd European Conference on Space Debris, Vol. 473, 2001, pp. 373–378.

[9] B. Bastida Virgili, DELTA debris environment long-term analysis, in: Proceedings of the 6th International Conference on Astrodynamics Tools and Techniques, ICATT, 2016.

[10] F. Letizia, B. Bastida Virgili, S. Lemmens, Assessment of orbital capacity thresholds through long-term simulations of the debris environment, Adv. Space Res. (2022) http://dx.doi.org/10.1016/j.asr.2022.06.010, URL https://www.sciencedirect.com/science/article/pii/S0273117722004793.

[11] J.C. Liou, LEGEND – a three-dimensional LEO-to-GEO debris evolutionary model, Adv. Space Res. 34 (2004) 981–986, http://dx.doi.org/10.1016/J.ASR.2003.02.027.

[12] J. Radtke, S. Mueller, V. Schaus, E. Stoll, LUCA2 - An enhanced long-term utility for collision analysis, in: Proceedings of the 6th European Conference on Space Debris, 2017, URL https://api.semanticscholar.org/CorpusID:59437355.

[13] J.C. Dolado-Perez, R. Di-Costanzo, B. Revelin, Introducing MEDEE - A new Orbital Debris Evolutionary Model, in: Proceedings of the 6th European Conference on Space Debris, 2013.

[14] K. Satomi, N. Nobuaki, T. Hanada, A. Shuji, Evaluation of active debris removal strategy using a debris evolutionary model, in: 70th International Astronautical Congress, 2019.

[15] A. Rossi, L. Anselmo, C. Pardini, R. Jehn, G. Valsecchi, The new space debris mitigation (SDM 4.0) long term evolution code, in: Proceedings of the 5th European Conference on Space Debris, 2009.

[16] A. Rossi, A. Cordelli, P. Farinella, L. Anselmo, C. Pardini, Long term evolution of the space debris population, Adv. Space Res. 19 (2) (1997) 331–340, http://dx.doi.org/10.1016/S0273-1177(97)00022-7, URL https://www.sciencedirect.com/science/article/pii/S0273117797000227, Space Debris.

[17] A. Rossi, L. Anselmo, A. Cordelli, P. Farinella, C. Pardini, Modelling the evolution of the space debris population, Planet. Space Sci. 46 (11) (1998) 1583–1596, http://dx.doi.org/10.1016/S0032-0633(98)00070-1, URL https://www.sciencedirect.com/science/article/pii/S0032063398000701, Second Italian Meeting on Celestial Mechanics.

[18] G.L. Somma, Adaptive remediation of the space debris environment using feedback control (Ph.D. thesis), University of Southampton, 2019, URL https://eprints.soton.ac.uk/447843/.

[19] A. D'Ambrosio, S. Servadio, P. Mun Siew, R. Linares, Novel source–sink model for space environment evolution with orbit capacity assessment, J. Spacecr. Rockets 60 (4) (2023) 1112–1126, http://dx.doi.org/10.2514/1.A35579.

[20] C.R. McInnes, An analytical model for the catastrophic production of orbital debris, ESA J. 17 (1993) 293–305.

[21] F. Letizia, C. Colombo, H.G. Lewis, Analytical model for the propagation of small-debris-object clouds after fragmentations, J. Guid. Control Dyn. 38 (2015) 1478–1491, http://dx.doi.org/10.2514/1.G000695.

[22] F. Letizia, C. Colombo, H. Lewis, Multidimensional extension of the continuity equation method for debris clouds evolution, Adv. Space Res. 57 (2015) 1624–1640, http://dx.doi.org/10.1016/j.asr.2015.11.035.

[23] S. Frey, Evolution and hazard analysis of orbital fragmentation continua (Ph.D. thesis), Politecnico di Milano, 2020.

[24] L. Giudici, M. Trisolini, C. Colombo, Probabilistic multi-dimensional debris cloud propagation subject to non-linear dynamics, Adv. Space Res. (2023) http://dx.doi.org/10.1016/j.asr.2023.04.030, URL https://www.sciencedirect.com/science/article/pii/S0273117723003083.

[25] C. Colombo, F. Letizia, H. Lewis, Spatial density approach for modelling of the space debris population, in: 26th AAS/AIAA Space Flight Mechanics Meeting, 2016, pp. 2749–2761.

[26] C. Duran, L. Giudici, C. Colombo, Modelling the Whole Space Debris Environment Through a Spatial Density Approach, in: 2021 AAS/AIAA Astrodynamics Specialist Conference, 2022, pp. 1–20.

[27] V. Braun, A. Horstmann, S. Lemmens, C. Wiedemann, L. Böttcher, Recent developments in space debris environment modelling, verification and validation with MASTER, in: Proceedings of the 8th European Conference on Space Debris, 2021.
[28] H. Klinkrad, DISCOS - ESA's database and information system characterising objects in space, Adv. Space Res. 11 (12) (1991) 43–52, http://dx.doi.org/10.1016/0273-1177(91)90541-Q, URL https://www.sciencedirect.com/science/article/pii/027311779190541Q.
[29] C. Hernández De La Torre, F. Pina Caballero, N. Sánchez Ortiz, H. Sdunnus, H. Klinkrad, DISCOS database and Web interface, in: Proceedings of the 3th European Conference on Space Debris, 2001.
[30] F. Jhon, J.P. LaSalle, L. Sirovich, Partial Differential Equations, fourth ed., Springer, New York, 1981.
[31] R.J. Leveque, Finite-Volume Methods for Hyperbolic Problems, Cambridge University Press, Cambridge, 2002.
[32] F. Letizia, Extension of the Density Approach for Debris Cloud Propagation, J. Guid. Control Dyn. 41 (12) (2018) 2651–2657, http://dx.doi.org/10.2514/1.G003675.
[33] S. Frey, C. Colombo, S. Lemmens, Extension of the king-hele orbit contraction method for accurate, semi-analytical propagation of non-circular orbits, Adv. Space Res. 64 (2019) 1–17, http://dx.doi.org/10.1016/j.asr.2019.03.016.
[34] L.G. Jacchia, Thermospheric temperature, density, and composition: New models, SAO Special Rep. 375 (1977).
[35] D. King-Hele, Theory of Satellite Orbits in An Atmosphere, Butterworhts Mathematical Text, London, 1964.
[36] L. Giudici, M. Trisolini, C. Colombo, Phase space description of the debris cloud dynamics through a continuum approach, in: 73rd International Astronautical Congress, 2022.
[37] M. Ananthasayanam, A. Anilkumar, P.S. Rao, New approach for the evolution and expansion of space debris scenario, J. Spacecr. Rockets 43 (6) (2006) 1271–1282, http://dx.doi.org/10.2514/1.19623.
[38] L. Giudici, C. Colombo, Space debris density propagation through a finite volume method, in: 33rd AAS/AIAA Space Flight Mechanics Meeting, 2023.
[39] M. Arioli, B. Codenotti, C. Fassino, The padé method for computing the matrix exponential, Linear Algebra Appl. 240 (1996) 111–130, http://dx.doi.org/10.1016/0024-3795(94)00190-1, URL https://www.sciencedirect.com/science/article/pii/0024379594001901.
[40] E.L. Kaplan, P. Meier, Nonparametric estimation from incomplete observations, J. Amer. Statist. Assoc. 53 (282) (1958) 457–481, http://dx.doi.org/10.1080/01621459.1958.10501452, URL https://www.tandfonline.com/doi/abs/10.1080/01621459.1958.10501452.
[41] F. Letizia, S. Lemmens, H. Krag, Environment capacity as an early mission design driver, Acta Astronaut. 173 (2020) 320–332, http://dx.doi.org/10.1016/j.actaastro.2020.04.041, URL https://www.sciencedirect.com/science/article/pii/S0094576520302459.
[42] C. Colombo, M. Trisolini, J.L. Gonzalo, L. Giudici, S. Frey, N.S. Ortiz, E.E. Kerr, F. Letizia, S. Lemmens, Design of a software to assess the impact of a space mission on the space environment, in: Proceedings of the 8th European Conference on Space Debris, 2021.
[43] M. Jankovic, M. Yüksel, M.M. Babr, F. Letizia, V. Braun, Space debris ontology for ADR capture methods selection, Acta Astronaut. 173 (2020) 56–68, http://dx.doi.org/10.1016/j.actaastro.2020.03.047, URL https://www.sciencedirect.com/science/article/pii/S0094576520301752.
[44] D. McKnight, A phased approach to collision hazard analysis, Adv. Space Res. 10 (1990) 385–388, http://dx.doi.org/10.1016/0273-1177(90)90374-9.
[45] L. Giudici, J.L. Gonzalo, C. Colombo, Density-based in-orbit collision risk model extension to any impact geometry, 2023, arXiv:2309.03562.
[46] O. Montenbruck, E. Gill, Satellite Orbits: Models, Methods and Applications, first ed., Springer Berlin, Heidelberg, 2000, http://dx.doi.org/10.1007/978-3-642-58351-3.
[47] L. Giudici, C. Colombo, M. Trisolini, J.L. Gonzalo, F. Letizia, S. Frey, Space debris cloud propagation through phase space domain binning, in: Aerospace Europe Conference, 2021.
[48] N.L. Johnson, P. Krisko, J.C. Liou, P. Anz-Meador, Nasa's new breakup model of evolve 4.0, Adv. Space Res. 28 (9) (2001) 1377–1384, http://dx.doi.org/10.1016/S0273-1177(01)00423-9.
[49] S. Frey, C. Colombo, Transformation of satellite breakup distribution for probabilistic orbital collision hazard analysis, J. Guid. Control Dyn. 44 (2021) 88–105, http://dx.doi.org/10.2514/1.G004939.
[50] J.L. Devore, N.B. Kenneth, Modern Mathematical Statistics with Applications, second ed., Springer New York, 2017, http://dx.doi.org/10.1007/978-1-4614-0391-3.
[51] J.C. Dolado-Perez, C. Pardini, L. Anselmo, Review of uncertainty sources affecting the long-term predictions of space debris evolutionary models, Acta Astronaut. 113 (2015) 51–65, http://dx.doi.org/10.1016/j.actaastro.2015.03.033, URL https://www.sciencedirect.com/science/article/pii/S0094576515001332.
[52] P.D. Anz-Meador, J.N. Opiela, D. Shoots, J.-C. Liou, History of On-Orbit Satellite Fragmentations 16th Edition Orbital Debris Program Office, Tech. rep, 2022, URL http://www.sti.nasa.gov.
[53] D.A. Vallado, W.D. McClain, Fundamentals of astrodynamics and applications, second ed., Springer, Dordrecht, 2007.
[54] J. Levandosky, First-Order Equations: Method of Characteristics, Stanford University, 2002, URL https://web.stanford.edu/class/math220a/handouts/firstorder.pdf.